The Journal of Undergraduate Research in Physics

CONTENTS

A CLUSTER ENUMERATION PROGRAM....................25

E. Sebastian Demme and Klaus Diemer
Köln, Federal Republic of Germany

CAPACITANCE-VOLTAGE CHARACTERISTICS OF THERMALLY OXIDIZED SILICON SUBSTRATES.....................27

John P. Culver
Louisiana State University

THE MANUFACTURE OF HEXADECANE FROM METHANOL: A FEASIBILITY STUDY.............................35

Christine A. Doyle
Creighton University

and

Susan Johnson
Oregon State University

DISTORTION OF SHADOWS IN NON-COHERENT LIGHT....39

Ravi Myneni
University of Louisville

VOLUME 3, NUMBER 2

WINTER 1984

Published by Guilford College
for
The American Institute of Physics and The Society of Physics Students

THE JOURNAL OF UNDERGRADUATE RESEARCH IN PHYSICS

This journal is devoted to research work done by undergraduate students in physics and its related fields. It is to be a vehicle for the exchange of ideas and information by undergraduate students. Information for students wishing to submit manuscripts for possible inclusion in the Journal follows.

ELIGIBILITY

The author must have performed all work reported in the paper as an undergraduate. The subject matter of the paper is open to any area of pure or applied physics or physics related field.

SPONSORSHIP

Each paper must be sponsored by a full-time faculty member of the department in which the research was done. A letter from the sponsor to the editor must accompany the manuscript if it is to be considered for publication.

FORM

The manuscript should be typed, double spaced, on 8 1/2 x 11 inch sheets. Margins of about 1 1/2 inch should be left on the top, sides, and bottom of each page. Papers should be limited to twelve pages of text in addition to an abstract and appropriate drawings, pictures, and tables.

GENERAL STYLE

All papers must conform to the Style Manual of the American Institute of Physics. Each paper must be prefaced by an abstract that does not exceed 250 words.

ILLUSTRATIONS

Line drawings should be made with black India ink on plain white paper. If a graph is drawn on co-ordinate paper, the paper must be lined blue. Important lines should be ruled in black. Each figure or table must be on a separate sheet. Photographs must have a high gloss finish.

CAPTIONS

A brief caption should be provided for each illustration or table, but it should not be part of the figure. They should be listed together at the end of the manuscript.

EQUATIONS

Equations should appear on separate lines and may be written in black India ink.

FOOTNOTES

Footnotes should be typed double spaced and grouped together in sequence at the end of the manuscript.

SUBMISSION

Two copies of the manuscript should be sent to:
Dr. Rexford E. Adelberger, Editor
THE JOURNAL OF UNDERGRADUATE RESEARCH IN PHYSICS
Physics Department
Guilford College
Greensboro, NC 27410

SUBSCRIPTION INFORMATION

The Journal will be published biannually with issues appearing in April and October of each year. There will be two issues per volume.

TYPE OF SUBSCRIBER	PRICE PER VOLUME
Individual	$ 5.00
Institution	$10.00

Foreign subscribers add $2.00 for postage

To receive a subscription, send your name, address, and check made out to The Journal of Undergraduate Research in Physics (JURP) to:

Journal of Undergraduate Research in Physics
Physics Department
Guilford College
Greensboro, NC 27410

BACK ISSUES

Back issues may be purchased by sending $10.00 per volume to the editorial office.

ISSN 0731 - 3764

The Journal of Undergraduate Research in Physics is published by Guilford College for the American Insititute of Physics and the Society of Physics Students.

A CLUSTER ENUMERATION PROGRAM

E. Sebastian Demme
Alte Fischenicher Str. 27, 5000 Köln 50
Federal Republic of Germany

and

Klaus Diemer
Curtiusstr. 8, 5000 Köln 41
Federal Republic of Germany

ABSTRACT

To count cluster configurations on a lattice, a FORTRAN program was developed which runs three times faster than previously published methods.

INTRODUCTION

For a long time, cluster enumeration has been a classic example that shows that from a mathematical point of view, many problems in physics are not completely solved (1). Since problems in percolation theory have become popular, interest in enumeration techniques has increased. Because of the early work in cluster enumeration, there already exist some algorithms (2,3) for enumerating isolated clusters on a regular lattice. A simple FORTRAN program published by S. Redner (2) used one of these algorithms for counting lattice animals (clusters) in two dimensions. The object of the algorithm is to determine the number of different cluster configurations consisting of n sites. As an example, for n = 3, there are only six different configurations (Figure 1).

```
*   **   **   *    *   ***
*   *     *   **   **
*
```

FIGURE 1
The six different cluster configurations where n = 3 on a regular lattice.

Thus, a correct computer program for calculating lattice animals has to give the result 6 for a cluster size of n = 3.

Starting independently of published methods, we succeeded in developing a faster algorithm for solving this problem. In this paper, we provide and discuss our FORTRAN program for cluster enumeration and try to explain why our algorithm is faster than Martin's (3) or Redner's (2).

THE ALGORITHM

We use the one-dimensional array IOCC to store the entire lattice. We initialized it as a 20 x 20 grid to ensure the enumeration of clusters up to a size of 20 sites. The neighbors of a site located at n are n+1, n-1, n+20, and n-20. These four directions are stored in location IV. They determine the structure of the lattice. Changing them enables us to enumerate clusters of more complex lattices. They are also called lattice animals (2) or fixed polyominoes (4). In IOCC, perimeter sites are symbolized by 0 and the free unoccupied lattice sites by 1. As every cluster site must have been a perimeter before it was added to the cluster, it is not necessary to differentiate between perimeters and cluster sites in IOCC.

To understand the algorithm, it is necessary to know how the number of perimeters (the number of empty neighbors of the cluster sites) of a cluster depends upon the number of perimeters of this cluster after reducing its size by one site. It is easier to look at this problem the other way around. If a cluster which consists of n sites and has p perimeters is enlarged by one site, the new (n+1) cluster has (p-1) perimeters plus the free neighbors of the added site. Free neighbors

are, in this context, unoccupied lattice sites which have not been perimeters of the old cluster.

We used a method similar to Redner (2) to build each configuration only once. After completion of a cluster of size n, the number of all locations where the (n+1)th cluster site is allowed to be placed is determined and stored in location IPER(n+1) (lines 20-30). As IPER(n+1) depends very much on IPER(n), it has to be updated every time the n-th cluster site is set (line 13). If a cluster consisting of NMAX-1 sites is built, it is not necessary to construct all configurations of the NMAX clusters which base on this NMAX-1 cluster and count them (as the Redner program does). By determining IPER(NMAX), we get this number easier and faster. So, we have only to construct all configurations up to the NMAX-1 cluster size. As this number of configurations in a square lattice is approximately a factor of 4 less than the number of all confifurations, our program runs four times faster than Redner's (2), despite the cost of initializing and updating IPER.

THE PROGRAM

The previous algorithm (2,3) is shorter and perhaps easier to understand as it actually builds each configuration. Hence, that method may be more useful for analyzing the structure and form of some configurations. On the other hand, our technique is four times faster.

The program (see Table 1) is written in simple FORTRAN which should run with most FORTRAN compilers. Using a FORTRAN IV compiler on the CYBER 176 at the University of Köln, the program requires approximately 49 sec of cpu time to enumerated all clusters of up to a size of 15. This represents a cluster counting rate of about 7.61×10^5 configurations per second. Redner's program (2), under similar conditions, produces a counting rate of 1.75×10^5 configurations per second.

REFERENCES

(1) Guttmann, A.J., Journal of Physics A, 15, 1987, (1982).

(2) Redner, S., Journal of Statistical Physics, 29, 309, (1982).

(3) Martin, J.L., Phase Transitions and Critical Phenomena, Vol. 3, C.Domb and M.S. Greed, Eds., Academic Press, New York, (1972), p. 97.

(4) Redelmeier, D.H., Discrete Mathematics, 36, 191, (1981).

FACULTY SPONSOR OF THIS PAPER
Professor D. Stauffer
Institute of Theoretical Physics
University of Köln
5000 Köln 41
Federal Republic of Germany

```
1        DIMENSION NE(20),JJ(20),JN(20),IPER(20),NUMB(20),IV(4),
        1 JP(4,20),IOCC(400)
2        DATA NMAX,N,NUMB(2),NE(1),JJ(2),IPER(2),JN(2),JP(1,1),
        1 JP (2,1),IOCC/13,5*2,1,22,41,22*0,378*1/,IV/1,20,-1,-20/
3        IOCC(41)=0
4  1     IF(IPER(N).GT.0) GO TO 3
5        IF(N.EQ.1) GO TO 8
6        N=N-1
7        J1=NE(N)
8        IF(J1.EQ.0) GO TO 1
9        DO 2 K=1,J1
10 2     IOCC(JP(K,N))=1
11       GO TO 1
12 3     ILOC=JP(JJ(N),JN(N))
13       IPER(N)=IPER(N)-1
14       JJ(N)=JJ(N)-1
15       IF(JJ(N).GT.0) GO TO 4
16       K=JN(N)
17       JN(N)=JN(K)
18       JJ(N)=JJ(K)
19 4     IF(N.EQ.NMAX-1) GO TO 7
20       NEIGH=0
21       DO 5 K=1,4
22       J1=ILOC+IV(K)
23       J2=IOCC(J1)
24       IOCC(J1)=0
25       JP(NEIGH+1,N)=J1*J2
26 5     NEIGH=NEIGH+J2
27       NE(N)=NEIGH
28       NM1=N
29       N=N+1
30       IPER(N)=IPER(NM1)+NEIGH
31       NUMB(N)=NUMB(N)+IPER(N)
32       IF(NEIGH.GT.0) GO TO 6
33       JJ(N)=JJ(NM1)
34       JN(N)=JN(NM1)
35       GO TO 1
36 6     JJ(N)=NEIGH
37       JN(N)=NM1
38       GO TO 1
39 7     NUMB(NMAX)=NUMB(NMAX)+IPER(N)+IOCC(ILOC+IV(1))+
        1 IOCC(ILOC+IV(2))+IOCC(ILOC+IV(3))+IOCC(ILOC+IV(4))
40       GO TO 1
41 8     WRITE(6,10) (NUMB(K),K=2,NMAX)
42 10    FORMAT(1X,7I11)
43       STOP
44       END
```

TABLE 1
FORTRAN listing of a program to enumerate the number of different cluster configurations on a regular lattice. This program can calculate for clusters up to n=20.

CAPACITANCE-VOLTAGE CHARACTERISTICS OF THERMALLY OXIDIZED SILICON SUBSTRATES

John P. Culver
Physics Department
Louisiana State University
Baton Rouge, LA 70803

ABSTRACT

An apparatus for thermally oxidizing silicon substrates was designed and constructed. Thermal oxidation occurs at appreciable rates when a substrate is exposed to an oxygen atmosphere at a temperature of about 1000 C. After oxidizing the substrate to the desired film thickness, aluminum contacts were placed on the surface by vapor deposition. This metal-oxide semiconductor (MOS) structure formed a nonlinear capacitor whose capacitance was a function of the applied voltage. Capacitance-voltage measurements were taken to determine the characteristics of this MOS device.

INTRODUCTION

The process used in the production of computer chips can be outlined as follows:

1. growing an oxide layer(s) into a silicon substrate;
2. coating the oxidized layer with a photoresist chemical;
3. photographing the circuit onto the coated substrate;
4. chemically etching the unexposed (photographically) photoresist;
5. chemically etching the exposed (visible) oxide;
6. diffusion of dopants into the removed oxide areas;
7. repetition of steps 1 - 6 until the desired circuit is obtained;
8. deposition of ohmic contacts and device connections.

In the finished product, a maze of transistors, diodes, resistors and capacitors abound. To produce the first three of these components, a bit of expertise and access to some elaborate equipment is required. To produce a capacitor, however, one grows an oxide film into the substrate surface by thermal oxidation, and then deposits metal contacts onto the surface of the oxide by vapor deposition. This relatively simple metal-oxide semiconductor structure forms a MOS capacitor.

To produce a MOS capacitor, a silicon substrate was placed in an oxygen atmosphere oven to speed up the thermal oxidation process:

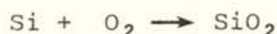

$$Si + O_2 \longrightarrow SiO_2$$

The contacts were made by depositing aluminum on the oxide by vapor deposition. A mask was used to regulate where the metal was deposited on the oxidized substrate. Capacitance-Voltage measurements were then taken to determine some of the inherent characteristics of this MOS capacitor.

PHYSICS OF THERMAL OXIDATION

Thermal oxidation is a common technique utilized in the electronics industry. This is done by placing silicon in an oxygen environment. Upon reaching the substrate surface, the oxygen molecules diffuse across the oxide layer and react at the oxide-silicon interface. The chemical reaction is either:

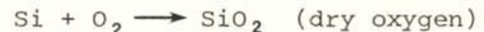

$$Si + O_2 \longrightarrow SiO_2 \quad \text{(dry oxygen)}$$

or

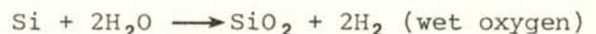

$$Si + 2H_2O \longrightarrow SiO_2 + 2H_2 \quad \text{(wet oxygen)}$$

A model for the oxidation process is shown in Figure 1. It is a plot of the concentration vs position across the silicon substrate. In the steady state, the flux through the gas-oxide interface, through the oxide, and across the oxide-silicon interface should all be equal. Using this, one can derive a relationship between the thickness of the oxide film and the time spent in the oxygen atomsphere.

The flux F_1 is proportional to the difference in concentrations of the oxygen in the gas and at the substrate surface:

$$F_1 = h_g(C_g - C_s) \qquad (1)$$

where h_g is the constant of proportionality defined as the mass transfer coefficient. Henry's Law states that in equilibrium, the concentration of a gas in a solution is directly proportional to the partial

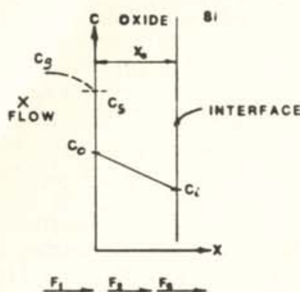

Figure 1
Concentration vs. Position for the silicon substrate. C_s is the oxygen concentration in the gas, C_o the concentration at the gas-oxide interface, $C_g$the concentration just below the oxide surface, and C_i is the concentration at the oxide-silicon interface.

pressure of that gas at the surface of the solution. Therefore, the concentration just below the surface is:

$$C_g = HP_s \qquad (2)$$

where H is Henry's constant and P_s the partial pressure. Likewise, the concentration in the oxide layer is given by:

$$C = HP_g \qquad (3)$$

The ideal gas equation is:

$$P = CkT \qquad (4)$$

Where C is the concentration of the gas, k the Boltzmann constant, and T the absolute temperature.

Combining the previous three equations gives:

$$F_1 = h_g (C - C_g)/(HkT) \qquad (5)$$

The flux (F_2) through the oxide layer is a diffusive flux. It can be represented as:

$$F_2 = D(C_o - C_i)/X_o \qquad (6)$$

where D is the diffusivity of the oxygen in the silicon dioxide and X_o is the thickness of the oxide.

The flux (F_3) through the oxide-silicon interface is proportional to the concentration at the interface:

$$F_3 = k_i C_i \qquad (7)$$

where k_i is the chemical surface reaction rate constant.

The film thickness growth rate is given by:

$$F = N(dx/dt) \qquad (8)$$

where N is the number of oxygen molecules/volume incorporated into the oxide layer. Recalling that all three fluxes are equal in the steady state, the flux in terms of gas concentration, known constants, and oxide thickness is given by the differential equation:

$$N\frac{dx}{dt} = \left[\frac{C}{\frac{1}{k_i} + \frac{HkT}{h_g} + \frac{x}{D}}\right] \qquad (9)$$

The general solution to this equation is:

$$x^2 + Ax = Bt \qquad (10)$$

where

$$A = 2D(1/k_i + HkT/h_g)$$

$$B = 2DC/N.$$

These constants are functions of temperature. Their values can be determined from the graphs in Figure 2.

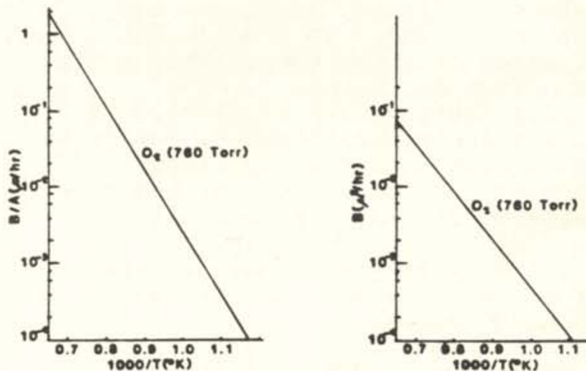

Figure 2
Temperature dependence of the constants A and B used to determine the time-thickness relationship.

Equation 10 can be rewritten to show the time required to grow an oxide layer of desired thickness:

$$t = (x^2 + Ax)/B \qquad (11)$$

APPARATUS

The Oven

The oxidation takes place in a special furnace. The major components are a quartz tube axially surrounded by a resistance furnace as shown in Figure 3. The furnace was heated to 1000 C and

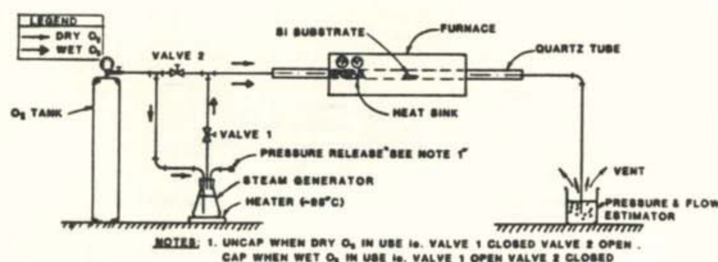

Figure 3
Schematic diagram of the apparatus used to oxidize silicon substrates.

welding oxygen passed through the tube at a flow rate of 1 cm/s. (Welding oxygen is a far cry from industrial grade oxygen, but will produce results that compare well with the theory.) After steady state was achieved, a sample was inserted through the end of the tube, placing it approximately at the center (lengthwise). The sample was oxidized for a predetermined amount of time to obtain a desired oxide thickness. This thickness was measured accurately by ellipsometry and approximately by the color of the film.

The growth was initiated with dry oxygen by having valve 1 (see Figure 3) closed and valve 2 open. At the intermediate state, valve 2 was closed and valve 1 opened. This forced the oxygen to filter through the water (about 95 C). At the final state, the procedure is terminated with dry oxygen.

The initial growth is rapid in dry oxygen (1) and then decreases as time proceeds. The component labeled "heat sink" is composed of quartz rods axially aligned with respect to the tube. These rods are small enough in diameter (about 1/8" for 1" diameter tube) to constrict the flow for a long enough time to allow the temperature of the gas to achieve equilibrium with the temperature of the furnace.

During the experiment, it was observed that the oxide growth rate varied as a function of the height from the bottom of the tube to the substrate surface. When a sample was placed near the bottom of the tube, the growth rate was faster than when placed near the center of the tube. The explanation of this has to do with the flow of the gas through the tube. When fluid flows through a circular tube, the velocity variation through a cross-section is maximum at the center, decreasing radially outward, approaching zero at the walls (see Figure 4). Samples placed at the bottom experience a slower and more uniform flow than those

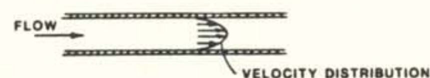

Figure 4
The velocity profile of the oxygen in the tube. This radial dependence causes the concentration of oxygen to vary with distance from the walls.

placed at the center. So, the concentration varies with the distance away from the center of the tube. The concentration must be higher at the walls because the growth rate is larger.

Vapor Deposition

The aluminum contacts were deposited on the oxide layer by vapor deposition with the aid of a mask. A

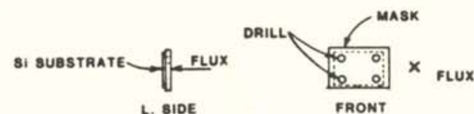

Figure 5
Shape of mask used when depositing the aluminum contacts

rectangularly shaped piece of metal was used to make the mask. The mask was slightly larger than the sample and had holes that allowed the metal vapor to be deposited on specific areas (see Figure 5) while shielding the remaining portion of the sample. Vapor deposition was performed in an evaporator that had a vacuum at a base

pressure of about 10^{-7} Torr (see Figure 6). The thickness of the deposited material is given by:

$$T = M/(2\pi R^2 \rho)$$

where M is the mass of aluminum in the boat of the evaporator, ρ is the density of alunimum and R is the distance from the sample surface to the boat. To ensure uniform thickness, the mask should be made as shown in Figure 7. The dimension L should be much less than the diameter to minimize diffraction of the incoming metal flux.

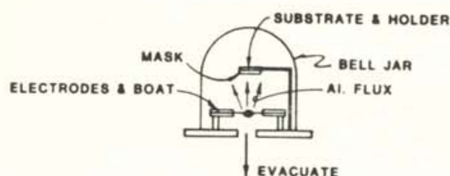

Figure 6
Schematic outline of the evaporator used to deposit the aluminum contacts on the silicon substrate.

The calculated amount of aluminum is placed in the tungsten boat. The system is evacuated to the specified pressure, and a 10-15 Amp current is passed through the boat, causing the aluminum to vaporize in the radial

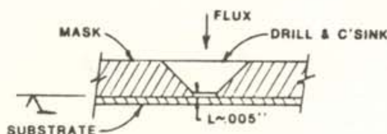

Figure 7
Cross section of the mask used when depositing the aluminum contacts.

direction. To ensure a good bond at the metal-oxide interface, the sample should be preheated by radiant heat from the boat before vaporization.

Capacitance Measurement

Two different schemes were used to measure how the capacitance depends on the applied voltage. The first was used for frequencies on the order of 0.1 Hz while the other was for frequencies on the order of one megahertz. Both use a quasistatic technique (2). At low frequencies, the capacitance of a MOS is directly proportional to the displacement current. As shown in Figure 8, the low frequency is generated by a ramp generator with a sweep rate of a few millivolts to 4 volts per second. The capacitance can be determined from the displacement current by:

$$i_d(V)\Big|_{V_0} = C(V)\Big|_{V_0} (dV/dt)$$

where dV/dt is the sweep rate of the generator and is a constant. The displacement current is on the order of

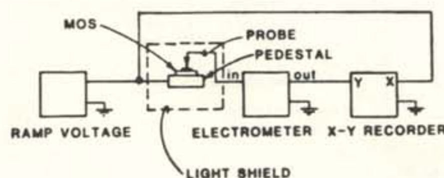

Figure 8
Schematic of the circuit used for the low frequency Capacitance-Voltage measurements.

nanoamps, so an electrometer was used to measure it. The electrometer amplifies the output voltage of the MOS such that:

$$i_d = -V_0/R_s$$

where R_s is the resistance setting of the electrometer. Calculating the displacement current at a particular input voltage, one can obtain the capacitance as a function of the applied voltage at low frequencies:

$$C(V_i) = i(V_i)/(dV/dt)$$

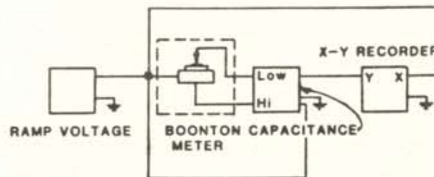

Figure 9
Schematic of the circuit used for the high frequency C-V measurements

At high frequencies, the electrometer is replaced by a Boonton capacitance meter. This instrument digitally displays the numerical values of the capacitance as the biasing voltage varies. A schematic of this setup is shown in Figure 9. The driving voltage was run at a frequency of 1 Mhz and an RMS value of 15 mV. A more complete description of the quasistatic technique can be found elsewhere (2).

Sample Preparation

A crucial part of this experiment is cleanliness. It cannot be overemphasized. Scrupulous care must be used to clean properly all interior surfaces. Two cleaning solutions (3) were used. All water used should be distilled and de-ionized. During the cleaning and experimental process, surgical gloves should be worn to prevent contamination of the apparatus or substrate. Sodium greatly alters the characteristics of the substrate. The oils and perspiration from one's fingers can have a profound effect on the quality of the film.

Good electrical contact is another important point. A dust particle between the substrate and the pedestal is sufficient to cause poor electrical contact. To check for proper electrical contact, the high frequency test is used. The value of the capacitance is measured in the strong accumulation region and compared with that calculated for a parallel plate capacitor. If there is poor electrical contact, the measured value of the capacitance will be much less than the calculated value.

RESULTS

Oxidation thickness-time

The time required to obtain different film thicknesses was calculated using Equation 11. Substrates were placed in the oven for these calculated times and the film thicknesses measured by ellipsometry. Table 1 shows these results. The 1000 Angstrom thickness film was obtained by exposing the silicon substrate to 1 atmosphere oxygen at 1000 C for about 2 hours. The results in Table 1 show good agreement between the theory and this experiment.

Capacitance-Voltage

Aside from determining the capacitance as a function of the applied voltage, high and low frequency plots (Figure 10) provide a quick qualitative description of the internal nature of the MOS structure. The threshold voltage, oxide capacitance, depletion capacitance, interfacial traps and the presence of ionic contamination are some of the immediate observations.

OXIDATION TIME (hr)	DESIRED* THICKNESS (Å)	ELLIPSOMETRY THICKNESS (Å)	COLOR OF OXIDE
.875	500	550	Brown
1.64	800	864	Blue
2.25	1000	1123	Violet
3.315	1300	1411	Blue-Violet

*Data based on A = .125 x 10^{-6} μ and B = .01 μ^2/hr for 1000°C at 760 torr.

Table 1

Results of thickness measurements. The times were determined by solving Equation 11 for the desired thickness of the oxide layer.

To obtain a C-V plot, the device is biased into accumulation and an AC signal is superimposed on top of this DC bias. The varying signal sweeps the device's charged state from accumulation through depletion and into strong inversion. Accumulation is the pile-up of majority charge carriers at the oxide-semiconductor interface. The accumulation capacitance is that of a parallel plate capacitor:

$$C_{acc} = C_{oxide} = \epsilon A/x_0$$

where ϵ is the permittivity of the oxide, A the area of the plates, and x_0 the thickness of the oxide.

As the AC signal is applied, majority charge carriers are repelled at the oxide-semiconductor interface and the charge state approaches depletion. In depletion, the majority charge carriers are depleted in a narrow region below the interface. This depleted region acts as a second dielectric. The total capacitance is the series combination of the oxide and the depleted semiconductor capacitances:

$$C_{dep} = C_0 C_S/(C_0 + C_S) \; ; \; C_S = \epsilon_S A/w$$

where C_0 is the oxide capacitance, C_S the semiconductor capacitance, ϵ_S the permittivity of silicon, A the field plate area, and w the depletion depth.

With a constant oxide capacitance, C_{dep} is a minimum when C_s is a minimum or when the depletion depth is a maximum. This variation accounts for the observed dip in the low frequency plot of Figure 10.

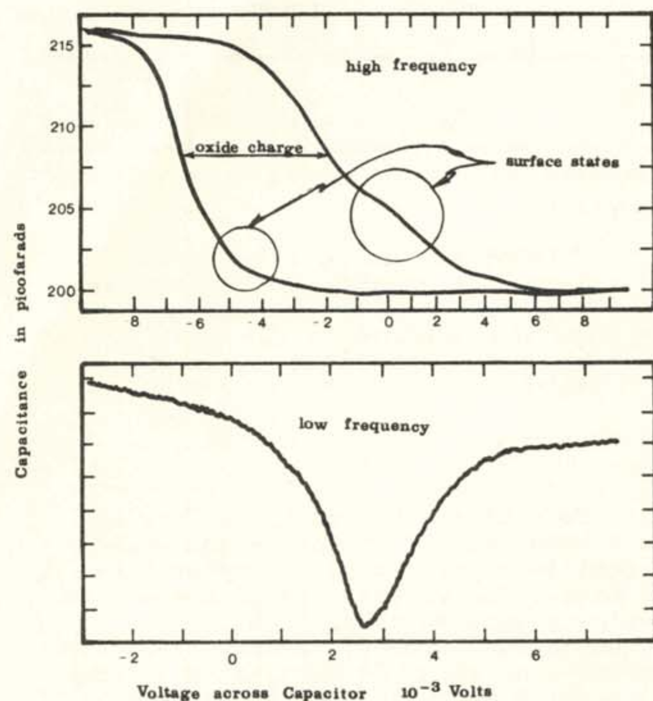

Figure 10
Typical C-V plots for boron doped silicon p-type substrates. The high frequency curves show the oxide charges and surface states.

Biasing the device beyond depletion brings its charged state into inversion. When the minority carrier concentration exceeds the majority carrier concentration, the device is said to be inverted. This inverted region lies just below the oxide, but is only a fraction of the depletion width. The measured capacitance may vary between two extremes. If the frequency of the test signal is low ($\omega \rightarrow 0$), the measured capacitance will be just the oxide capacitance. One can view the biasing as a succession of DC states since the time between consecutive levels is long compared to the recombination-generation rate. For low frequency tests, minority charges pile up just below the oxide-semiconductor interface. This situation is analogous to accumulation so,

$$C_{acc} = C_{inv}$$

On the other hand, if the frequency is high ($\omega \rightarrow \infty$), the relatively slow recombination-generation rate can not supply minority charge build-up at the oxide-semiconductor interface. Instead, the charge piles up at the edge of the depletion width. This situation is analogous to the depletion case yeilding:

$$C_{inv} = C_{dep}$$

This is independent of the applied DC bias.

Ideally, the traces for high frequency plots are identical when sweeping the device from accumulation to inversion and then from inversion to accumulation. Figure 10 indicates that this is not the case with our system.

In early studies of MOS devices, deviations from the ideal model were placed into four major catagories:

1. work-function difference;
2. mobile ions in the oxide;
3. fixed oxide charge;
4. interfacial traps.

The work-function is defined as the minimum energy required to raise an electron in a metal from the Fermi level to infinity. The work-function difference is the difference between the work-function for the metal field plate and that of the doped semiconductor. The effect of the work-function difference is to cause the C-V plot to translate along the horizontal axis.

Secondly, the presence of mobile ions in the oxide was discovered. These ions enter the oxide by contamination from alkali metals (usually sodium). Ionic contamination will also cause the C-V plots to translate along the voltage axis, especially during elevated temperatures. The amount of translation is dependent on the location and concentration within the oxide. In this experiment, the sweeps were carried out continuously. Thus the hysteresis displayed in Figure 10 is not the result of ionic contamination.

A popular method for de-mobilizing the ions is chlorine neutralization.

During the oxidation process, chlorine is introduced into the ambient. A highly concentrated chlorine material forms near the oxide-semiconductor interface. The alkali ions wander into this newly formed material and are traped and neutralized by the chlorine. This eliminates these ionic effects.

Even when these findings were incorporated into the ideal model, there were still perplexing deviations from laboratory results. To find the answer, thin layers of the oxide were etched away. Each layer was examined with photomeasurements. Excess ionic silicon was identified and given the name fixed oxide charge. These charge sites reside near the oxide-semiconductor interface. Before silicon reacts with oxygen, the atoms must be broken away from the silicon substrate. When the oxidation process is terminated, these uncompensated atoms give rise to charge sites. These sites also cause a translation in the C-V plot. This effect can be minimized by annealing the oxide in an inert gas or by terminating the oxidation process with dry oxygen at 1200 C. Both yield the same minimal density, but inert gas annealing requires lower temperatures (600-1200 C).

The hysteresis displayed by Figure 10 is due to interfacial traps. Interfacial traps are the result of silicon atoms with one valence electron unbonded (known as dangling bonds). If a silicon crystal is cleaved along a particular atomic plane, the exposed surface will be a plane of dangling bonds since adjacent atoms are bonded covalently. Some of these dangling bonds will react with oxygen atoms. The atomic spacing of the oxygen atoms in silicon dioxide, however, dictates that some of the dangling bonds will be left "dangling". These remaining unreacted bonds form the interfacial traps.

During biasing, the density of the interfacial traps varies with the applied voltage. At one extreme (accumulation or inversion), the traps may be filled. At the other extreme, the traps may be empty. Therefore, these traps may aid or oppose the applied bias for opposite sweep directions. Interfacial traps also distort the C-V plots such as the rolling contours seen on the high frequency plots. To minimize the density of these traps, the device is annealed in hydrogen. The atomic hydrogen attaches itself to the dangling bonds, thereby neutralizing the trap.

C-V plots are a convenient means for revealing the internal structure of a MOS device. High and low frequency plots assist in analyzing the structure and characterizing deviations from the ideal model. The underlying causes can be identified and then eliminated or minimized. Although a theoretical curve was not established, the theoretical threshold voltage can be used as a reference point to investigate the work-function difference, the mobile ions, and the oxide charge.

SUMMARY

This experiment was the result of a one semester project, but it is advisable to spend one semester perfecting the process for producing MOS capacitors and one semester analyzing the devices. Annealing procedures can be easily incorporated into the system. These will help to identify the deviations from the ideal model. If elipsometry can be used to accurately determine the oxide thickness, the oxidation system can be characterized for film growth rates. The most important features of the system are the heat sink (to ensure that the temperature of the gas is in equilibrium with the temperature of the furnace) and the pressure-flow estimator (to establish atmospheric pressure throughout the system and to estimate the flow rate. After building the system and before growing oxides, the system should be flushed out with oxygen with the furnace on, thereby removing any remaining contaminants.

ACKNOWLEDGEMENTS

The author would like to thank John Mitchelle of the Physics Department and Dr. Burke Huner of the Electrical Engineering Department for their help and the suggestion that made this experiment possible.

REFERENCES

(1) A.S. Grove, Physics and Technology of Semiconductor Devices, 1st ed., John Wiley & Sons, 1967 pp 22-32.

(2) A.D. Lopez, The Review of Scientific Instruments, 44, 2, February 1973, pp 200-204.

(3) W. Kern, "Cleaning Solutions Based on Hydrogen Peroxide for use in Silicon Semiconductor Technology", RCA Review 31, June 1970, pp 187-206.

FACULTY SPONSOR OF THIS PAPER
Dr. Paul Kirk
Physics Department
Louisiana State University
Baton Rouge, LA 70803

THE MANUFACTURE OF HEXADECANE FROM METHANOL: A FEASIBILITY STUDY

Christine A. Doyle
The Medical School
Creighton University
Omaha, NE 68178

and

Susan Johnson
Nuclear Engineering Department
Oregon State University
Corvallis, OR 97331

ABSTRACT

This study explores the thermodynamic feasibility of manufacturing hexadecane from methyl alcohol for use as diesel fuel. The study shows that such a procedure is possible using off-the-shelf equipment and existing technology. Useable by-products are water, sodium hydroxide and chlorine gas. The heat source is a small nuclear reactor. Design figures for a 1000 liter/day plant indicate an overall efficiency of 27%.

INTRODUCTION

The inevitable exhaustion of fossil fuel supplies has drawn attention to alternate sources of energy for the operation of our transportation systems. In the case of the private automobile, the work has focused chiefly upon the substitution of ethanol for octane as the chemical fuel. Ethanol, like octane, is a liquid and therefore convenient to handle. It is easily obtained and when used in an internal combustion engine, does not pollute as heavily as octane. It is a "clean" fuel.

There are, however, some difficulties in using ethanol as a motor fuel. Ethanol has an energy content of 2.68×10^4 J/gm, while octane delivers 4.44×10^4J/gm (1). This means that a vehicle would have to carry more weight of fuel to obtain the same range if it were to burn ethanol instead of octane. Ethanol, as a motor fuel, causes corrosion problems which manifest themselves in more and higher repair costs. Finally, the use of ethanol raises the question if plant life should be used for food or fuel. These points diminish the attractiveness of ethanol as a fuel.

Methanol is an even worse motor fuel. However, it is possible to synthesize from methanol a quite suitable diesel fuel which could be utilized by a large portion of the present transportation fleet. Since methanol is abundant and easily obtainable from many varied sources, the question of food versus fuel does not arise. Since a significant portion of the fleet presently in use is designed to burn diesel fuel, conversion to this fuel would not require the rebuilding which would be necessary if ethanol became the new standard fuel.

This proposal for the synthesis of hexadecane from methanol has two major sections. The first describes the chemical reaction which synthesizes the hexadecane and the second the design parameters for a pilot plant.

THE CHEMICAL REACTION

The chemical reaction relies primarily on the Wurtz reaction (2) to convert methanol into hexadecane via the sodium organometallic compound in five recursive steps (Figure 1). The advantages of this synthetic route include the speed of the reaction and the symmetric straight chain nature of the product. Another advantage is the tolerance of impurities in the feedstock. The overall reaction is endothermic, requiring an energy input of 6.42×10^5 J/mole of hexadecane produced. To make the reaction take place, however, one must supply 7.77×10^6 J/mole. Of this energy, 7.14×10^6 J/mole is returned as heat and the rest taken up in the hexadecane and the

by-products. The reaction will proceed at an adequate rate at 373 K (room temperature). The choice of NaCl as the reagent was made on the grounds of its availability.

```
1)  16 MeOH + 16 NaCl ==> 16 MeCl + 16 NaOH
2)  16 MeCl + 16 NaOH + 8 H2 ==> 8 Ethane + 16 NaCl + 16 H2O
3)  8 Ethane + 4 Cl2 ==> 8 EtCl + 4 H2
4)  8 EtCl + 8 NaOH + 4 H2 ==> 4 Butane + 8 NaCl + 8 H2O
5)  4 Butane + 2 Cl2 ==> 4 ButCl + 2 H2
6)  4 ButCl + 4 NaOH + 2 H2 ==> 2 Octane + 4 NaCl + 4 H2O
7)  2 Octane + Cl2 ==> 2 OctCl + H2
8)  2 OctCl + 2 NaOH + H2 ==> Hexadecane + 2 NaCl + 2 H2O
```

FIGURE 1
A schematic of the Wurtz Reaction that produces hexadecane from methanol.

The methanol for the procedure was produced in a still. The initial feedstock consisisted of 10% methanol and 90% water. These figures are a reasonable output of a fermentation process. The still had an 80% recovery rate and produced a stream of 80% methanol and 20% water at 1 atmosphere and 331 K. This stream must be raised to 373 K and injected into the Wurtz reaction process.

The reaction requires chlorine and hydrogen gas. Therefore, the NaCl must be electrolysed to produce them. This adds a further energy requirement to make the reaction occur.

DESIGN

We propose to use as the energy source a nuclear reactor which was originally designed for use in an electric powered space probe (3). It can provide 1.2×10^6 Wt at 1400 K with a lifetime of 7 years and a reliability of .95 (4). The package was designed to drive a thermoelectric module producting 1×10^5 We with a hot shoe temperataure of 1400 K and a cold shoe temperature of 775 K (3). In our proposal, the reactor has been derated to 8×10^2 Wt with an operating temperature of 1400 K. The thermoelectric converter was kept to electrolyse the NaCl, but with a cold shoe temperature of 700 K.

The operating temperature of the chemical converter is 373 K, so rather than waste this high grade energy, a conventional steam generator was inserted into the system (Figure 2). The steam generator was of a saturated steam design to eliminate problems associated with superheating the steam. Steam tables (5) give an operating pressure of 2.4×10^7 Pa at an input temperature of 680 K. This stage of the system will recover 2.33×10^5 We and will reject 4.67×10^5 Wt at 373 K (Table 1).

THE ENERGY BUDGET

For a system that produces 1000 liters (6150 moles) per day of hexadecane, the chemical conversion module requires 1.66×10^5Wt for the reaction, 5.3×10^4Wt for the operation of the still and 1.41×10^5We to electrolyse the NaCl.

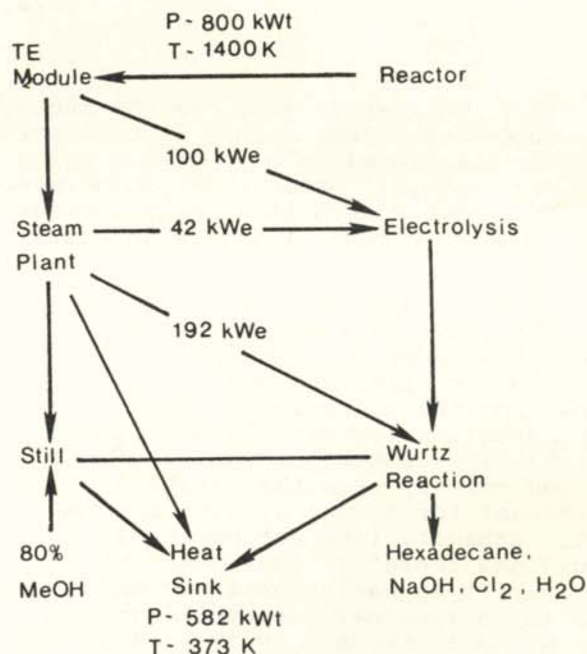

FIGURE 2
Overall plant schematic for the production of hexadecane from methanol.

The overall energy budget for this system (Table 2) shows a return of 2.7×10^5 We plus 10^3 liter/day of hexadecane, and 4.57×10^5Wt at 373 K. This low quality energy can be used for hot water supply, space heating, or other things.

Ignoring losses in the system from conduction paths out of the system (everything is well insulated) and possible schemes for recovering the low grade energy, the system has an overall energy recovery efficiency of 27%. The efficiency, when considering only the

energy taken up in the hexadecane production, is 3%. A reasonable assumption for fuel efficiency in a vehicle is 8 Km/l. A plant as we propose would provide fuel for 8000 vehicle kilometers per day.

Plant design	Saturated steam
Operating temperature	680 K
Operating pressure	24 MPa
Turbine type	Multistage impulse
Input temperature	700 K
Reject temperature	373 K
Thermal power temperature	700 kWt
Rejected power output	467 kWt
Electrical power output	233 kWt
Carnot efficiency	0.467
Assumed mechanical efficiency	0.75
Assumed electrical efficiency	0.95
Overall efficiency	0.33

TABLE 1
Schedule for the steam plant to be used as an energy supply.

CONCLUSION

The Wurtz synthesis of hexadecane is both technically and economically feasible. The overall efficiency of 27% is quite reasonable and compares well with the efficiency of the same components when used only to generate electricity. The design is straight forward. The system is essentially catalytic. Therefore, it seem that implementation and further study is warranted.

REFERENCES

(1) "Enthalpies of Combustion at One Atmosphere, 25 Centigrade", Selected Values of Properties of Hydrocarbons, National Bureau of Standards Circular No. C461, Washington DC, 1947.

(2) Morrison, R.T., and R.N. Boyd, Organic Chemistry, Allyn & Bacon, Inc., Newton, MA, 1983, p. 100.

(3) Mondt, J.F., and G. Stapfer, "Nuclear Power Source for Electric Propulsion", Jet Propulsion Laboratories, California Institute of Technology, Pasadena, CA, 1979.

(4) Buden, D., "100-kWe Nuclear Space Electric Power Source", Los Alamos Scientific Laboratory, Los Alamos, NM, 1979.

(5) CRC Handbook of Chemistry and Physics, 60th Ed., CRC Press, Boca Raton, FL, 1980, p. xxx.

FACULTY SPONSOR OF THIS PAPER
Dr. Philip T. McCormick
Department of Physics
The University of Santa Clara
Santa Clara, CA 95053

Module	Item	Power/Temp
Reactor	Power out	800 kWt
	Temperature out	1400 K
Thermoelectric module	Power in	800 kWt
	Temperature in	1400 K
	Power out	100 kWe
	Power rejected	800 kWt
	Rejection temp.	700 K
Steam plant	Power in	700 kWt
	Temperature in	700 K
	Power out	233 kWe
	Power rejected	467 kWt
	Rejection temp.	373 K
Chemical process	Power in	166.34 kWt
	Still power	52.96 kWt
	Electrolysis	140.97 kWe
Total, power out	Electrical	192.05 kWe
	Enthalpy	25.39 kW
	Waste (heat sink)	582.56 kWt
	Total	800.00 kW
Overall Recovery Efficiency		27.2%

TABLE 2
Overall power budget for the synthesis of hexadecane.

DISTORTION OF SHADOWS CAST IN NON-COHERENT LIGHT

Ravi Myneni
Department of Physics
University of Louisville
Louisville, KY 40292

ABSTRACT

Two occulting screens, placed at different heights and close in separation, produce a striking effect of distorting the shadow of the lower screen. By means of a computer simulation, we were able to account for this effect.

INTRODUCTION

On a sunny day, one can readily observe a peculiar and striking effect of shadow distortion by placing two occulting screens at different heights, but with a small horizontal separation, in the light of the sun. In such a situation, the shadow of the lower screen extends noticeably beyond its normal position. Figure 1 shows the shadows cast by a rectangular screen (semi-infinite plane) and a disk shaped screen placed in the sun light. The rectangular screen is placed closer to the image plane than the disk shaped one. Notice how the shadow of the rectangular screen is distorted.

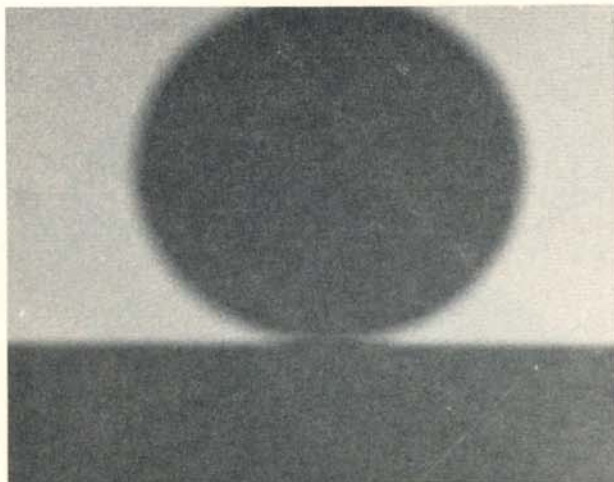

Figure 1
The shadow of the lower screen (semi-infinite plane) is distorted when the upper screen (disk) is positioned next to it. The source of light is the sun.

The usual reaction to this phenomenon is to interpret this effect of shadow distortion in terms of diffraction or interference. Since the sun light is incoherent, the explanation must lie elsewhere. The intensity distribution is found in this case by averaging over the phases.

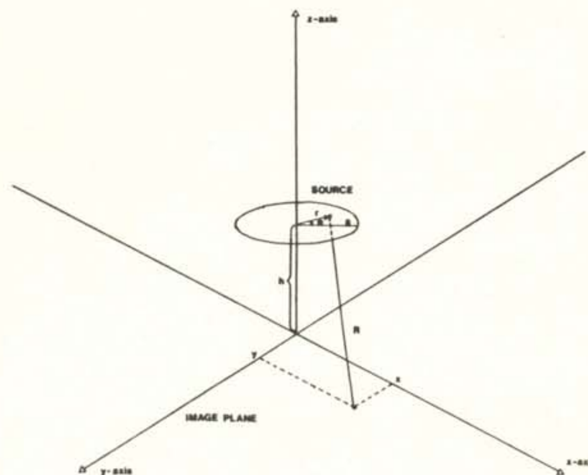

FIGURE 2
A disk shaped source illuminates the image plane without obstruction.

CALCULATION OF IMAGE PATTERN

To determine the light intensity in the image plane, we use the technique of ray tracing. Consider the case of a circular light source without any obstruction as depicted in Figure 2.

Since the source is incoherent, the intensity at a point (x,y) in the image plane is the sum of the contributions from all points on the source, independent of phase. Thus:

$$I(x,y) = \iint_{source} \frac{N \; r \; dr \; d\theta}{R^2} \qquad (1)$$

where N is the radiance, (r,θ) locates the source point, and $R^2 = (r\cos\theta - x)^2 + (r\sin\theta - y)^2 + h^2$

The effect of an obstructing screen (see Figure 3) is to impose specific limits on the integral in Equation 1. The only source points that contribute to a point in the image plane are those that are exposed. If the points under consideration are close to the origin and a h, then, as a first approximation, we may assume that R~h. Further, if the source is of uniform intensity, N is constant and can be removed from the integral. The resulting approximation for Equation 1 is:

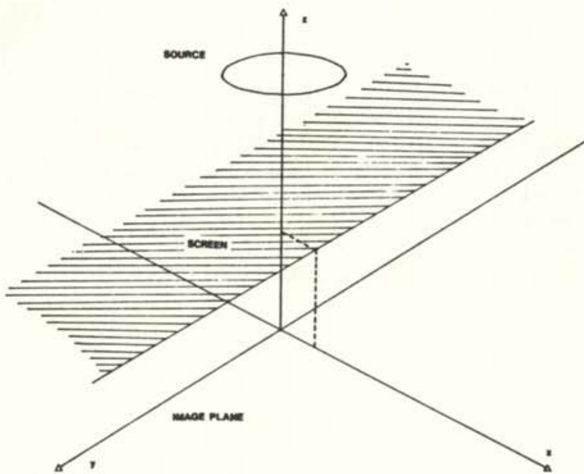

FIGURE 3
A semi-infinite screen obstructs the disk shaped source.

$$I(x,y) = \frac{N}{h^2} \iint_{\text{exposed region of source}} r \; dr \; d\theta \qquad (2)$$

The integral part of Equation 2 is simply the amount of surface area as seen from a point in the image plane. Our computer simulation was developed to calculate this surface area exactly, from point to point. The resulting intensity curves were then plotted.

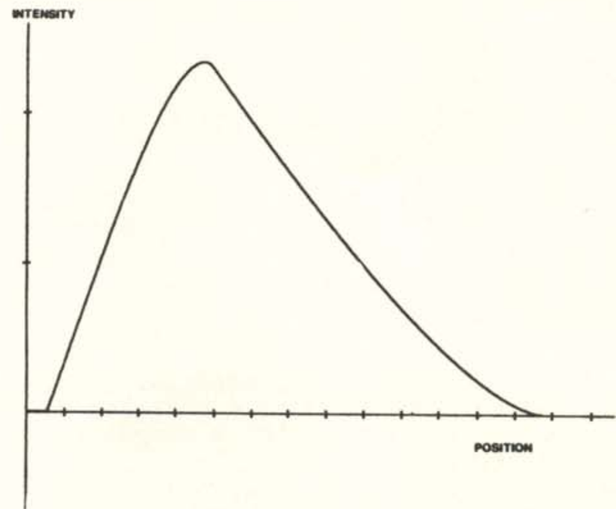

FIGURE 4
Plot of the intensity along the x-axis for a single occulting screen.

RESULTS OF THE SIMULATION

For the case of with a single occulting screen (Figure 3), the intensity curve along the x-axis is shown in Figure 4. This curve

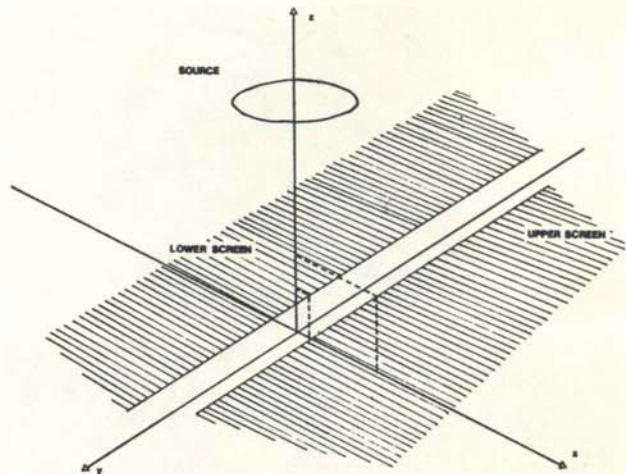

FIGURE 5
Two screens at different heights and with a small horizontal separation (x) obstructs the source.

corresponds well to the more precise theoretical values (1). For the case with two obstructing screens at different heights (Figure 5), our computer simulation yielded the intensity curve shown in Figure 6. The result of superimposing all three curves is shown in Figure 7. This figure clearly reveals a displacement between the x-intercept of the intensity curve for the lower screen alone (point A), and that for both screens (point B). It is this displacement which appears as an extension of the shadow of the lower screen. Thus, by using the technique of ray tracing, we were able to simulate this experiment and to account for this striking effect of shadow distortion.

ACKNOWLEDGMENTS

The author is indebted to Professor Gwinn for invaluable assistance.

REFERENCES

(1) Considine, Philip S., J. Opt. Soc. Am., 56, 8 (1966).

FACULTY SPONSOR OF THIS PAPER

Dr. J. A. Gwinn
Department of Physics
University of Louisville
Louisville, KY 40292

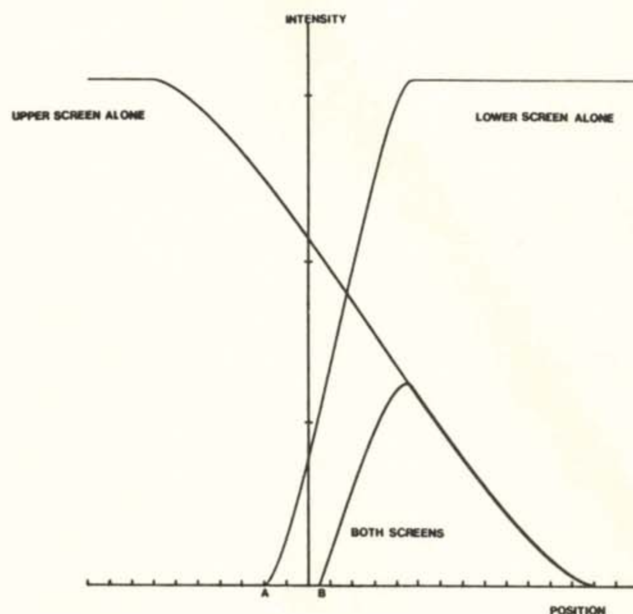

FIGURE 7
Superposition of the intensity curves for the three situations reveals a shift in the beginning of the shadow of the lower screen.

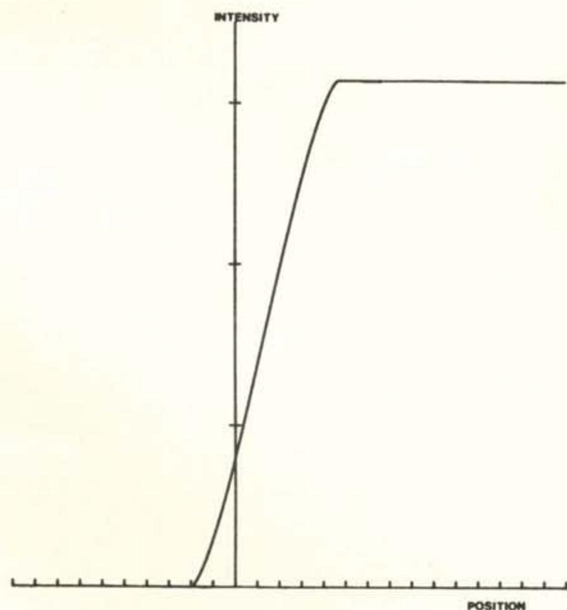

FIGURE 6
Plot of the intensity along the x-axis for the two occulting screens shown in Figure 5.